Synthesis and Characterization of Self-Assembled Polyaniline Nanotubes/Silica Nanocomposites

Gordana Ćirić-Marjanović,*,† Ljiljana Dragičević,† Maja Milojević,† Miloš Mojović,† Slavko Mentus,† Biljana Dojčinović,‡ Budimir Marjanović,§ and Jaroslav Stejskal‖

Faculty of Physical Chemistry, University of Belgrade, Studentski trg 12-16, 11158 Belgrade, Serbia; Department of Chemistry, ICTM, Njegoševa 12, 11001, Belgrade, Serbia; Centrohem, Vuka Karadžića bb, 22300 Stara Pazova, Serbia; and Institute of Macromolecular Chemistry, Academy of Sciences of the Czech Republic, 162 06 Prague 6, Czech Republic

Received: January 5, 2009; Revised Manuscript Received: March 9, 2009

Self-assembled semiconducting, paramagnetic polyaniline nanotubes have been synthesized by the oxidative polymerization of aniline with ammonium peroxydisulfate in aqueous medium in the presence of colloidal silica particles of an average diameter ~12 nm, without added acid. The electrical conductivity of polyaniline nanotubes/silica nanocomposites is in the range $(3.3-4.0) \times 10^{-3}$ S cm^{-1}. The presence of paramagnetic polaronic emeraldine salt form of polyaniline and phenazine units in nanocomposites was proved by FTIR, Raman, and EPR spectroscopies. The influence of the initial silica/aniline weight ratio on the morphology of polyaniline/silica nanocomposites was studied by scanning and transmission electron microscopies. Nanocomposites synthesized by using the initial weight ratio silica/aniline ≤0.2 contain polyaniline nanotubes which have a typical outer diameter of 100−250 nm and an inner diameter of 10−80 nm, and nanorods with a diameter of 60−100 nm, accompanied with polyaniline/silica nanogranules, while the nanocomposite synthesized at weight ratio silica/aniline ~2 contains polyaniline/silica nanogranules with an average diameter of 35−70 nm. The evolution of molecular and supramolecular structure of polyaniline in the presence of colloidal silica is discussed.

Introduction

Polyaniline (PANI) is one of the most extensively studied conducting polymers because of its simple synthesis[1] and doping/dedoping chemistry,[2] low cost, high conductivity, excellent environmental stability, and wide potential applicability[3,4] in rechargeable batteries, erasable optical information storage, shielding of electromagnetic interference, microwave and radar absorbing materials, sensors, indicators, catalysts, electronic and bioelectronic components, membranes, electrochemical capacitors, electrochromic devices, nonlinear optical and light-emitting devices, electromechanical actuators, and antistatic and anticorrosion coatings. Its electromagnetic and optical properties depend mostly on its oxidation state and protonation degree.[5] The green emeraldine salt form $[(-B-NH^{\cdot+}-B-NH-)_n](A^-)_n$ is conducting (~10 S cm^{-1}), while the emeraldine base form $[(-B-N=Q=N-)_n(-B-NH-)_{2n}]$, the leucoemeraldine base form $[(-B-NH-)_n]$, the pernigraniline base form $[(-B-N=Q=N-)_n]$, and the pernigraniline salt form $[(-B-NH^+=Q=NH^+-)_n](A^-)_n$ are nonconducting, where B, Q, and A^- denote a benzenoid unit, quinonoid unit, and dopant anion, respectively. The preparation of bulk quantities of conducting granular PANI is usually performed by the oxidative polymerization of aniline with ammonium peroxydisulfate (APS) in an acidic aqueous solution (initial pH < 2.0).[1]

At the present time, conducting PANI nanostructures (nanofibers, nanorods, nanotubes, etc.) are the focus of intense research owing to their significantly improved dispersibility and processability, and substantially enhanced performance in many applications in comparison with granular PANI.[6] It has recently been recognized that the oxidation of aniline with APS in aqueous solution, starting at pH > 4.0 and finishing at pH < 2.0 (a falling pH method), is a reliable template-free synthetic route to PANI nanotubes.[7−19] Conducting self-assembled PANI nanotubes have been successfully synthesized in the presence of various inorganic acids,[7] sulfonic acids,[8,9] carboxylic acids,[10−13] polymeric acids,[14] sulfonated carbon nanotubes,[15] sulfonated dendrons,[16] and titanium dioxide.[17] The new simplified template-free (STF) method of the synthesis of conducting PANI nanotubes, by the oxidation of aniline with APS in water without any added acid, has recently been proposed.[11,18] The reliability of STF method has been proved in follow-up studies.[19]

Nowadays, syntheses of new conducting polymer composites with improved mechanical properties, processability, or heat resistance in comparison to corresponding pure conducting polymers alone, as well as the studies of their electrical, optical, magnetic, and catalytic properties, constitute a great scientific challenge. Extensive research in a broad field of synthesis and characterization of nanomaterials composed from inorganic nanoparticles and conducting polymers develops intensively, with the aim to design and prepare nanocomposites with the efficient interaction between the conjugated polymeric matrix and inorganic nanoparticles, leading thus to the fabrication of nanomaterials with unique physicochemical properties and applicability. PANI/silica (PANISIL) composites have received growing attention during past two decades.[20−45] PANISIL composites have been prepared by the chemical[20,22,24−26,28,31,33,35,37−39,41,42,45] and electrochemical[23,29,32,34,43] oxidative polymerization of aniline in the presence of silica (mainly colloidal silica), sol−gel synthesis,[21,27,30,40,44] plasma polymer-

* Corresponding author. E-mail: gordana@ffh.bg.ac.yu.
† University of Belgrade.
‡ ICTM.
§ Centrohem.
‖ Academy of Sciences of the Czech Republic.

10.1021/jp900096b CCC: $40.75
Published on Web 04/29/2009

ization,[36] and by the addition of silica to the PANI solution.[33] It was found that PANISIL nanocomposites have substantially improved properties, such as dispersibility and processability,[25] stability,[38] durability,[38] electrochromism,[38] and capacitance[43] of films, and are able to form considerably thinner and smoother films[25] in comparison with pure PANI. These hybrid materials were proposed to have potential applications as novel materials for recovery of precious metals and for catalytic applications,[24] for the asymmetric synthesis of chiral chemicals and for the ion-exchange separation of chiral anions,[23] as a cathode in lithium batteries,[29,32] as a membrane for direct methanol fuel cell,[40] in electrochromic devices,[38,42] and in high-pulse-power energy storage devices.[43]

It can be expected that the combination of desirable properties of PANI (good environmental stability, high electrical conductivity, electrochromism, reversible transformation of various oxidation states, catalytic, antistatic and anticorrosion activity) and silica (good heat resistance, high tensile strength, and hardness), together with unique properties of one-dimensional (1D) nanostructures of PANI, can lead to significant improvement of technological performance of new 1D PANISIL nanomaterals in comparison with standard granular PANI, 1D nanostructured PANI, and ordinary PANISIL composites. To the best of our knowledge, only a single study was devoted to the template-guided preparation of PANISIL nanotubes, by in situ polymerization of anilinium ion adsorbed on the surface of silica nanotubes, which acted as a template.[45] Here we report, for the first time, the template-free synthesis of conducting PANI nanotubes/silica nanocomposites by the STF method, which opens up a wide range of opportunities in the production of other nanocomposites of conducting self-assembled 1D PANI nanostructures and various inorganic materials. It should be noted that this facile synthetic method not only efficiently omits a hard template and post-treatment of template removal, but also simplifies the selection of reagents. Prepared PANISIL nanocomposites were characterized by FTIR, Raman, EPR, and ICP spectroscopies, scanning (SEM) and transmission (TEM) electron microscopies, thermogravimetric and elemental analysis, and electrical conductivity measurements. The influence of initial silica/aniline weight ratio on the molecular and supramolecular structure of synthesized PANISIL composites is reported in the present communication. The reaction kinetics, thermochemistry, and the mechanism of the oxidative polymerization of aniline in aqueous dispersion of colloidal silica, without added acid, are discussed. The thermochemistry of the studied polymerization processes was computationally modeled with semiempirical quantum chemical MNDO-PM3/COSMO method.[9,46−51]

Experimental Section

Materials. Aniline (p.a. >99.5%, Centrohem, Serbia) was distilled under reduced pressure and stored at room temperature, under argon, prior to use. APS (analytical grade, Centrohem, Serbia) and amorphous anhydrous colloidal silica (Aerosil 200, Degussa, average particle diameter ~12 nm) were used as received.

Synthesis of PANISIL Nanocomposites. Specified amount of colloidal silica (0.04, 0.40, or 4.0 g) was dispersed in distilled water (80 mL) and dispersion was homogenized by magnetic stirring for 15 min. Aniline (20 mmol, 1.86 g) was added to the above dispersion and then this solution was diluted with distilled water up to 100 mL. Aqueous solution of APS (0.25 M, 100 mL) was poured into the aqueous dispersion of aniline and silica. The reaction mixtures were stirred for 160 min at room temperature and then filtered. The PANISIL precipitates were rinsed with 0.005 M H_2SO_4 aqueous solution and dried in vacuum at 60 °C for 3 h. The initial pH values of aqueous dispersions of aniline and silica, containing 0.04, 0.4, and 4.0 g of silica, before addition of APS solution were 7.2, 7.1, and 6.5, respectively, and pH values of corresponding filtrates after polymerization were 1.7, 1.7, and 1.8, respectively. As a reference, PANI was prepared by the same procedure, in the absence of silica. In the following text, PANISIL nanocomposites, synthesized at the initial weight ratios of silica to aniline $w_{silica/aniline}$ ~0.02, 0.2, and 2, are labeled as PANISIL-1, PANISIL-2, and PANISIL-3, respectively, and corresponding deprotonated forms are denoted as PANISIL-D-1, PANISIL-D-2, and PANISIL-D-3. The deprotonation was performed by treating 1 g of nanocomposite with 100 mL of 5% ammonium hydroxide with stirring. The resulting deprotonated PANISIL nanocomposites were separated by filtration, rinsed with 5% ammonium hydroxide, and dried in vacuum at 60 °C for 3 h.

Characterization. Aniline adsorption on colloidal silica at room temperature, under conditions corresponding to the initial conditions of the syntheses of PANISIL-1, PANISIL-2, and PANISIL-3, without added APS, was analyzed using a UV−vis spectrometer GBC Cintra 10e. Specified amounts of anhydrous colloidal silica (0.04, 0.40, or 4.0 g) were dispersed in distilled water (80 mL) and the dispersions were homogenized by magnetic stirring for 15 min. Aniline (20 mmol, 1.86 g) was added and the dispersions were diluted with distilled water up to 200 mL. The resulting aqueous dispersions of aniline (0.1 M) and colloidal silica were allowed to equilibrate for 15 min under stirring and then filtered (filter paper Filtrak 390). All filtrates (the first 1 mL), as well as aqueous aniline solution (0.1 M) without added colloidal silica, were diluted (1000×) with distilled water prior to UV spectroscopy measurements. It should be noted that filtrates of aqueous dispersions of colloidal silica, without the addition of aniline, did not show any absorbance in the investigated wavelength region of 210−320 nm. The decrease of aniline concentration was determined by monitoring the decrease of absorbance at the wavelength of absorption maximum $\lambda_{max} = 230$ nm. The adsorption isotherm of aniline on colloidal silica, at room temperature, was determined as follows: anhydrous colloidal silica (1 g) was dispersed in distilled water (20 mL) and the dispersions were homogenized by magnetic stirring for 15 min. Aniline (0.5−15 mmol) was added and the dispersions were diluted with distilled water up to 50 mL. The resulting aqueous dispersions of aniline (0.01−0.3 M) and colloidal silica were allowed to equilibrate for 15 min under stirring and then filtered. The decrease of aniline concentration was determined by monitoring the decrease of absorbance at the wavelength of absorption maximum $\lambda_{max} = 230$ nm. Scanning electron microscope (SEM) JEOL JSM 6460 LV and a transmission electron microscope (TEM) Tecnai G2 Spirit (FEI, Brno, Czech Republic) have been used to characterize the morphology of the samples. Powdered materials were deposited on adhesive tape fixed to specimen tabs and then ion sputter coated with gold using a BAL-TEC SCD 005 Sputter Coater prior to SEM measurements. The thermogravimetric analysis was carried out using a TA Instruments Model SDT 2960 thermoanalytical device with either nitrogen or air purging gas, at a flow rate of 35 mL min^{-1} and at a heating rate of 10 °C min^{-1}. Elemental analysis (C, H, N, and S) was performed using an elemental analyzer Vario EL III (Elementar). The content of Si in the PANISIL composites was determined by inductively coupled plasma with optical emission spectroscopy (ICP-OES) technique, using a Thermo

Scientific iCAP 6500 Duo ICP spectrometer. The PANISIL sample was placed in a platinum crucible, and a PANI part of the composite was burned for 45 min using the Bunsen burner. The inorganic residue (silica) was fused with sodium carbonate (weight ratio Na_2CO_3/silica = 15) for 1 h, cooled to room temperature, dissolved in bidistilled water and analyzed by ICP at emission line of Si (212.4 nm). The conductivity of PANISIL powders compressed between stainless pistons was measured at room temperature by means of an ac bridge (Waynne Kerr Universal Bridge B 224), at fixed frequency of 1.0 kHz. During the measurement, pressure was maintained at 124 MPa. FTIR spectra of PANISIL powders dispersed in KBr pellets were recorded using a MIDAC M2000 SRL FTIR spectrometer at 2 cm^{-1} resolution in the range of 400−4000 cm^{-1}. Raman spectra excited with a diode-pumped solid-state high-brightness laser (532 nm) were collected on a Thermo Scientific DXR Raman microscope, equipped with a research optical microscope and a CCD detector. The laser beam was focused on the sample placed on an X−Y motorized sample stage using objective magnification ×50 (~1.1 μm laser spot size). The scattered light was analyzed by the spectrograph with a grating 900 lines mm^{-1}. Laser power was kept at 0.1 mW on the sample (PANISIL and PANI) in order to avoid its degradation. The EPR spectra of solid-state samples were obtained at room temperature using a Varian E104-A EPR spectrometer operating at X-band (9.3 GHz) using the following settings: 1 G modulation amplitude, 100 kHz modulation frequency, and 10 mW microwave power. Spectra were recorded and analyzed using EW software (Scientific Software).

Computational Method. The semiempirical MNDO-PM3 model[52] (included in molecular orbital package[53] MOPAC 97, part of the Chem3D Pro 5.0 package, CambridgeSoft Corp.), with full geometry optimization by the EigenFollowing procedure[54] were used to obtain the heat of formation (ΔH_f) of individual species. The conformational analysis of aniline oligomers was done. Input files for the semiempirical computations were the most stable conformers of the investigated molecular structures, with minimized steric energy using the MM2 molecular mechanics force-field method.[55] The COSMO technique has been applied during the geometry optimization to approximate the effect of a solvent surrounding the molecule.[56]

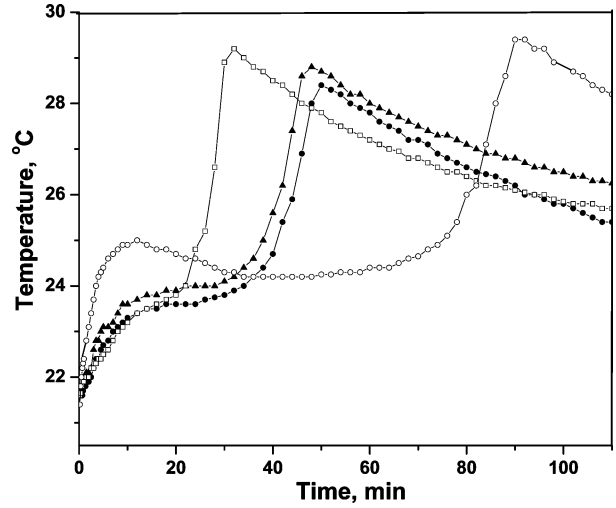

Figure 1. Temperature changes during the polymerization of aniline (0.1 M) with APS (0.125 M) in water: without added colloidal silica (○), and for the synthesis of PANISIL-1 (●), PANISIL-2 (▲), and PANISIL-3 (□) composites.

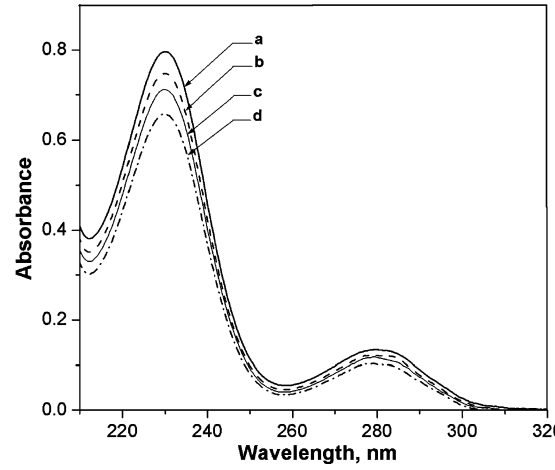

Figure 2. UV spectra of diluted (1000×) aqueous solutions of aniline (0.1 M, a), and filtered aqueous dispersions of aniline (0.1 M) and colloidal silica [0.2 g dm^{-3} (b), 2.0 g dm^{-3} (c), and 20.0 g dm^{-3} (d)], corresponding to the initial reaction conditions of the syntheses of PANISIL-1 (b), PANISIL-2 (c), and PANISIL-3 (d), without added APS.

Results and Discussion

Thermochemistry and Kinetics of Chemical Oxidative Polymerization of Aniline in Aqueous Dispersions of Colloidal Silica. The oxidation of aniline with APS in aqueous silica dispersions, without added acid, is an exothermic process (Figure 1). The silica/aniline weight ratio has significant influence on the kinetics and thermochemistry of this process. The syntheses of PANISIL-1 and PANISIL-2 proceed in two exothermic phases which are well separated by an athermal period (Figure 1), similarly to the corresponding oxidation of aniline in water,[11,18] while the synthesis of PANISIL-3 proceeds as an complex exothermic process, i.e., two rapid heat evolutions intercepted with slow heat evolution. The oxidative polymerization of aniline in aqueous dispersions of colloidal silica is completed considerably faster than in water without added colloidal silica. The reaction medium cools down after the temperature reached its maximum (postpolymerization period). The initial rate of aniline oxidation in aqueous silica dispersions is lower than the initial rate of aniline oxidation in water. The presence of colloidal silica also causes the decrease of the amount of heat released during the first exothermic phase of aniline polymerization. This is due to the decrease of the concentration of aniline molecules in the bulk of the aqueous silica dispersion, because of the partial adsorption of aniline molecules on colloidal silica particles. This adsorption is proved by the UV spectroscopy (Figure 2). The adsorption isotherm of aniline on colloidal silica in aqueous dispersion is shown in Figure 3. The more efficient adsorption of aniline during synthesis of PANISIL-3 was observed (0.1000 M → 0.0827 M; 17.3% adsorbed aniline), in comparison with the adsorption of aniline during syntheses of PANISIL-1 (0.1000 M → 0.0940 M; 6.0% adsorbed aniline) and PANISIL-2 (0.1000 M → 0.0894 M; 10.6% adsorbed aniline). It follows that the heterogeneous oxidation of aniline adsorbed on colloidal silica, besides the oxidation of dissolved aniline (homogeneous oxidation with APS and heterogeneous oxidation with precipitated pernigraniline-like oligoanilines and PANI), also occurs. Since the rates of the oxidation of dissolved and adsorbed aniline with APS, as well as with pernigraniline-like oligoanilines and PANI, are substantially different, the well-known semiempirical rate equation of the oxidative polymerization of aniline with APS in

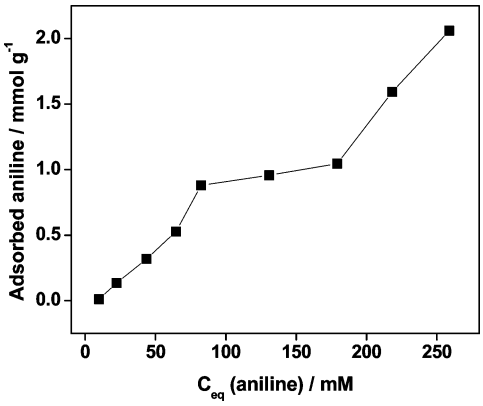

Figure 3. Adsorption isotherm of aniline adsorbed on colloidal silica in aqueous dispersion (C_{eq} denotes an equilibrium concentration of aniline in the solution obtained after filtration of the aqueous dispersion containing aniline and colloidal silica).

aqueous solution (eq I)[22c] became much more complex in the case of corresponding oxidation of aniline in aqueous colloidal silica dispersions without added acid (eq II):

$$-\mathrm{d[An]}/\mathrm{d}t = k_1[\mathrm{An}][\mathrm{APS}] + k_2[\mathrm{An}][\mathrm{P}] \quad \text{(I)}$$

$$-\mathrm{d[An]}/\mathrm{d}t = (k_1[\mathrm{APS}] + k_2[\mathrm{O}] + k_3[\mathrm{P}])[\mathrm{An}] + (k_1'[\mathrm{APS}] + k_2'[\mathrm{O}] + k_3'[\mathrm{P}])[\mathrm{An_{ads}}] \quad \text{(II)}$$

where [An], [An_{ads}], [APS], [O], and [P] are the concentrations of dissolved aniline, adsorbed aniline, APS, pernigraniline-like oligoaniline, and pernigraniline-like PANI, respectively, and k_1, k_1', k_2, k_2', k_3, and k_3' are rate constants. It is interesting to note here that Armes's group,[22c] in their study of the kinetics of polymerization of aniline in an acidic aqueous colloidal silica dispersion, has revealed the similar decrease of the initial rate of aniline oxidation with APS in the presence of colloidal silica. The neglect of the adsorption of aniline molecules on colloidal silica particles has led Armes's group to the conclusion that the presence of colloidal silica causes the significant decrease of k_1. Our results indicate that the [An] is significantly reduced, k_1 remains the same, and $k_1 > k_1'$. We propose that the mechanism and kinetics of the first exothermic polymerization phase is governed by the homogeneous oxidation of dissolved aniline in the case of PANISIL-1 synthesis, while the increase of silica/aniline weight ratio lead to the increased significance of the heterogeneous oxidation of adsorbed aniline, especially in the case of PANISIL-3 synthesis.

The nonprotonated aniline molecules are prevalent over anilinium cations ($pK_a = 4.6$) at the beginning of the oxidation (pH ~7). The fast oxidative oligomerization of nonprotonated aniline molecules, which are much more oxidizable than anilinium cations,[46−48] with peroxydisulfate is accompanied with rapid heat evolution, without an induction period characteristic for the oxidative polymerization of aniline in an acidic aqueous solutions.[11,48] It should be noted here that the aniline oligomerization (polymerization) itself is not exothermic but rather endothermic process. The driving force for the oxidative oligomerization (polymerization) of aniline is the exothermic reduction of the oxidant. Semiempirical quantum chemical MNDO-PM3/COSMO calculations indicate that the oxidative dimerization of aniline in aqueous silica dispersion at the initial pH ~7, leading to the formation of nonprotonated 4-aminodiphenylamine (4-ADPA) [pK_a(protonated 4-ADPA) = 5.2] and hydronium ions (half-reaction 1), occurs with the absorption of heat ($\Delta H_r = 251.6$ kcal mol^{-1}). The reductive transformation of peroxydisulfate to sulfate in aqueous solution (half-reaction 2) is accompanied with the heat release ($\Delta H_r = -297.8$ kcal mol^{-1}). The overall redox dimerization process (reaction 3) is thus exothermic ($\Delta H_r = -46.2$ kcal mol^{-1}). The oxidation of formed 4-ADPA with peroxydisulfate in aqueous solution (reaction 4), during the first exothermic phase of aniline polymerization, which leads to the formation of nonprotonated *N*-phenyl-1,4-benzoquinonediimine (B−*N*═Q═NH) and hydronium ions, is slightly exothermic process ($\Delta H_r = -8.3$ kcal mol^{-1}).

$$2C_6H_5NH_{2(aq)} + 2H_2O_{(aq)} \xrightarrow{-2e^-} \text{4-ADPA}_{(aq)} + 2H_3O^+_{(aq)} \quad (1)$$

$$S_2O_8{}^{2-}_{(aq)} \xrightarrow{+2e^-} 2SO_4{}^{2-}_{(aq)} \quad (2)$$

$$2C_6H_5NH_{2(aq)} + S_2O_8{}^{2-}_{(aq)} + 2H_2O_{(aq)} \rightarrow \text{4-ADPA}_{(aq)} + 2SO_4{}^{2-}_{(aq)} + 2H_3O^+_{(aq)} \quad (3)$$

$$\text{4-ADPA}_{(aq)} + S_2O_8{}^{2-}_{(aq)} + 2H_2O_{(aq)} \rightarrow \text{B—N═Q═NH}_{(aq)} + 2SO_4{}^{2-}_{(aq)} + 2H_3O^+_{(aq)} \quad (4)$$

The acidity of reaction mixture continuously increases because of the formation of hydronium ions as byproduct.[11,18] The exothermic protonation of hydrated aniline molecules, $\Delta H_r = -33.4$ kcal mol^{-1}, and primary amino groups of leucoemeraldine-like oligoanilines with released hydronium ions also contributes to the rapid heat evolution. The linear and branched oligoanilines are formed during the first exothermic polymerization phase (Figure 4).[18,46−48,57] The linear N−C4 coupled leucoemeraldine-like oligoanilines, being much more oxidizable than aniline monomer,[46−48] are easily oxidized with peroxydisulfate to protoemeraldine- [(−B—N═Q═N−)$_n$-(−B—NH−)$_{6n}$], emeraldine-, nigraniline- [(−B—N═Q═N−)$_{3n}$(−B—NH−)$_{2n}$], and pernigraniline-like nonprotonated oligoanilines. The oxidative intramolecular cyclization of branched oligoanilines with peroxydisulfate leads to the formation of substituted phenazines (pseudomauveine, etc., Figure 4).[18,46−48,57] The MNDO-PM3/COSMO computations confirm the exothermic nature of these oxidative oligomerization reactions of aniline with peroxydisulfate in water.

The concentration of peroxydisulfate rapidly decreases and the oxidized nonprotonated aniline oligomers, especially fully oxidized pernigraniline-like oligoanilines, are formed in substantial amount as insoluble precipitates (oligoaniline and silica/oligoaniline) during the first polymerization phase (Figure 4). We suppose that the weight ratio of oligoaniline to silica/oligoaniline precipitates decreases with the increase of the initial silica/aniline weight ratio. The concentration of nonprotonated aniline molecules also decreases, even more rapidly than APS, partly because of their oxidative oligomerization and partly because of the pH decrease. The decrease of pH from ~7 to 4.6 causes the decrease of the ratio [$C_6H_5NH_2$]/[$C_6H_5NH_3^+$] from ~300 to 1. Because the anilinium cation is much weaker reductant than nonprotonated aniline molecule,[46−48] and the nonprotonated pernigraniline-like oligoanilines are much weaker oxidants than peroxydisulfate, the oxidative polymerization of remaining $C_6H_5NH_2$/$C_6H_5NH_3^+$ shows considerable slowdown until it is almost stopped at pH ~3.5. At this point low-reactive anilinium cations became significantly prevalent over reactive nonprotonated aniline molecules [$C_6H_5NH_2$]/[$C_6H_5NH_3^+$] ~0.1 at pH ~3.5).

The reaction mechanism during the second (athermal) polymerization phase, Figure 1, is based on the very slow redox

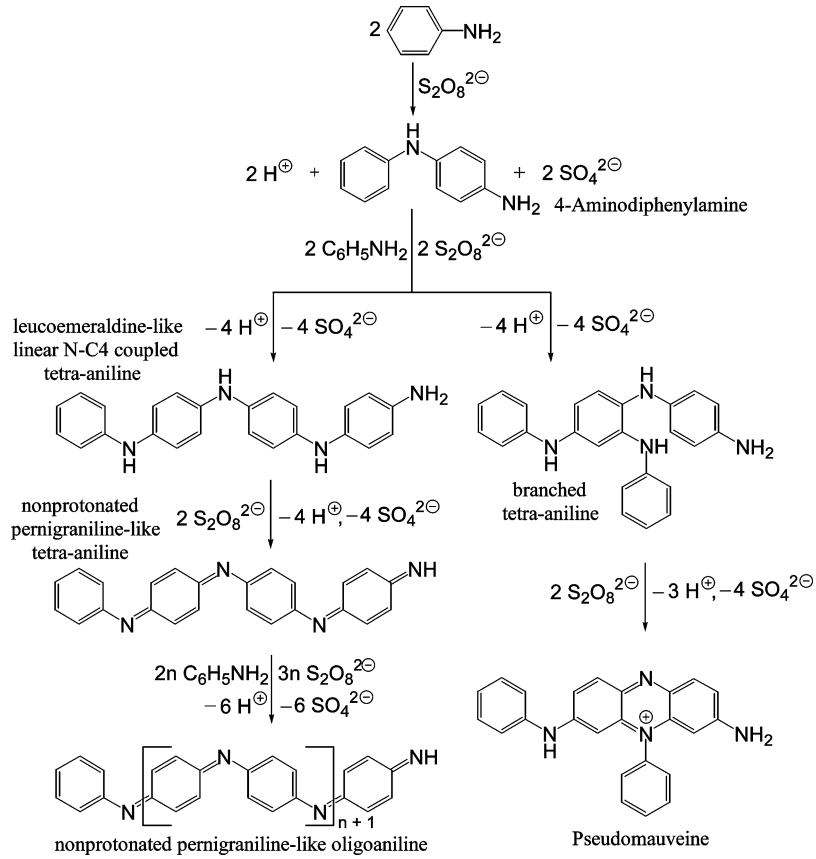

Figure 4. Mechanism of the first exothermic phase of the oxidative polymerization of aniline with APS, in aqueous dispersion of colloidal silica, without added acid.

processes: homogeneous oxidation of $C_6H_5NH_2/C_6H_5NH_3^+$ with remaining peroxydisulfate, reaction 5, and heterogeneous oxidation of $C_6H_5NH_2/C_6H_5NH_3^+$ with precipitated nonprotonated pernigraniline-like oligoanilines and peroxydisulfate leading to the growth of nonprotonated pernigraniline-like oligoanilines (reaction 6).

$$C_6H_5NH_3^+{}_{(aq)} + C_6H_5NH_{2(aq)} + 2S_2O_8^{2-}{}_{(aq)} + 5H_2O_{(aq)} \rightarrow B{-}N{=}Q{=}NH_{(aq)} + 4SO_4^{2-}{}_{(aq)} + 5H_3O^+{}_{(aq)} \quad (5)$$

$$C_6H_5NH_3^+{}_{(aq)} + C_6H_5NH_{2(aq)} + 3S_2O_8^{2-}{}_{(aq)} + B{-}(N{=}Q{=}N{-}B)_n{-}N{=}Q{=}NH_{(s)} + 7H_2O_{(aq)} \rightarrow B{-}(N{=}Q{=}N{-}B)_{n+1}{-}N{=}Q{=}NH_{(s)} + 6SO_4^{2-}{}_{(aq)} + 7H_3O^+{}_{(aq)} \quad (6)$$

It has recently been shown by Trchová et al. that the weight-average molecular weight of precipitated oligoanilines undergoes minor changes during the athermal period of the oxidation of aniline in water without added acid.[18] It can be concluded that the reaction 5 is the major redox process during this polymerization phase of the syntheses of PANISIL composites. The accumulation of B−N=Q=NH during the athermal period of the oxidation of aniline, with APS in water without added acid, was also tentatively proposed by Gospodinova et al.[58] From the mechanistic point of view, this phase is quite similar to the induction period of the oxidative polymerization of aniline which starts in an acidic aqueous solution, the difference only being the state of the protonation of B−N=Q=NH (nonprotonated, $B{-}N{=}Q{=}NH_2^+$ and $B{-}NH^+{=}Q{=}NH_2^+$).[46,48] During this second oxidation phase, the acidity slowly increases (pH 3.5 → 2.5), inducing thus further decrease of the $[C_6H_5NH_2]/[C_6H_5NH_3^+]$ ratio (0.1 → 0.01).

We have proved by the MNDO-PM3/COSMO computational method that the formation of B−N=Q=NH by the oxidation of $C_6H_5NH_2/C_6H_5NH_3^+$ with peroxydisulfate (reaction 5), as the main slow redox process during the second phase of aniline polymerization, is much less exothermic process ($\Delta H_r = -25.6$ kcal mol^{-1}) than the corresponding formation of B−N=Q=NH by the oxidation of nonprotonated aniline molecules ($\Delta H_r = -54.5$ kcal mol^{-1}) during the first exothermic polymerization phase. Taking into account that the rapid decrease of the concentration of $C_6H_5NH_2$, owing to the oxidative consumption of $C_6H_5NH_2$ at pH 3.5 → 2.5, is suppressed in considerable extent with the formation of $C_6H_5NH_2$ via the endothermic deprotonation ($\Delta H_r = 33.4$ kcal mol^{-1}) of prevalent low-reactive $C_6H_5NH_3^+$, the net thermochemical effect is nearly athermal second phase of PS-1 and PS-2 syntheses (Figure 1). The importance of endothermic hydrolytic processes on the thermochemistry of this polymerization phase should not be neglected.[58]

The presence of colloidal silica causes a significant acceleration of redox reactions during the second polymerization phase at pH < 3.5 (reaction 6), i.e., the much shorter athermal periods during the PANISIL-1 and PANISIL-2 syntheses, and the shortest slightly exothermic second period of PANISIL-3 synthesis, compared with the corresponding athermal period of synthesis of pure PANI, in water without added acid. This could be explained by the substantial increase of the surface area of precipitated oligoanilines in the presence of colloidal silica. The increase of the surface area of nigraniline- and pernigraniline-like oligoanilines causes the increase of k_2 and k_2', which are

composite quantities containing a contribution from the specific surface area of the precipitating oligoanilines.[22c]

The exothermic protonation of B−N=Q=$NH_{(aq)}$ (reaction 7, $\Delta H_r = -47.6$ kcal mol^{-1}), as well as the exothermic protonation of other fully oxidized pernigraniline-like oligoanilines (reaction 8), causes the significant increase of their oxidant power and solubility,[46,47] leading thus to the autoacceleration of aniline polymerization at pH < 2.5 (second exothermic phase of the PANISIL-1 and PANISIL-2 syntheses which took place after athermal polymerization phase, and the third exothermic phase of the PANISIL-3 synthesis, Figure 1).

$$\mathrm{B{-}N{=}Q{=}NH_{(aq)} + 2H_3O^+_{(aq)} \rightarrow B{-}NH^+{=}Q{=}NH_2{}^+_{(aq)} + 2H_2O_{(aq)}} \quad (7)$$

$$\mathrm{B{-}(N{=}Q{=}N{-}B)_n{-}N{=}Q{=}NH_{(s)} + 2(n+1)H_3O^+_{(aq)} \rightarrow B{-}(NH^+{=}Q{=}NH^+{-}B)_n{-}NH^+{=}Q{=}NH_2{}^+_{(s/aq)} + 2(n+1)H_2O_{(aq)}} \quad (8)$$

Protonated nigraniline- and pernigraniline-like oligoanilines as well as remaining peroxydisulfate react with remaining $C_6H_5NH_2/C_6H_5NH_3^+$ and reduced segments of partly oxidized oligoanilines, via the exothermic redox equilibrating process, leading thus to the formation of longer PANI chains in the form of emeraldine salt (PANI sulfate) with prevalent N−C4 coupling mode between aniline units. In this polymerization phase sulfate anions (pK_{a2} of sulfuric acid is ~2) became also exothermically protonated (reaction 9, $\Delta H_r = -27.0$ kcal mol^{-1}), thus promoting charge separation process in the emeraldine salt form of oligoanilines and PANI, i.e., formation of delocalized polaronic form of PANI hydrogen sulfate.[47,57]

$$\mathrm{SO_4{}^{2-}_{(aq)} + H_3O^+_{(aq)} \rightarrow HSO_4{}^-_{(aq)} + H_2O_{(aq)}} \quad (9)$$

From the mechanistic point of view, the exothermic third phase of the oxidative polymerization of aniline with APS in water without added acid, at pH < 2.5, is very similar to the single exothermic phase of the oxidative polymerization of anilinium sulfate with APS in an aqueous solution.[48] MNDO-PM3/COSMO computational method indicates that the oxidation of $C_6H_5NH_2/C_6H_5NH_3^+$ with protonated pernigraniline-like oligoanilines (reaction 10), which is accompanied with the release of hydronium ions, is an exothermic process.

$$\mathrm{(-NH^+{=}Q{=}NH^+{-}B{-})_{n(s/aq)} + xC_6H_5NH_{2(aq)} + yC_6H_5NH_3{}^+_{(aq)} + (2x+3y)H_2O_{(aq)} \rightarrow (-NH^+{=}Q{=}NH^+{-}B{-})_{n-x-y}\,(-NH{-}B{-})_{3x+3y(s/aq)} + (2x+3y)H_3O^+_{(aq)}} \quad (10)$$

Our MNDO-PM3/COSMO thermochemical computations, regarding the oxidative polymerization of aniline with APS in water without added acid (reaction 11), are proved to be in excellent agreement with the corresponding experimental thermochemical data obtained by Fu et al.[59] The enthalpy change measured by solution calorimetry (−105.0 kcal mol^{-1} of aniline)[59] at [APS]/[aniline] ≤ 1.25 corresponds well to the enthalpy change computed by MNDO-PM3/COSMO method (−103.5 kcal mol^{-1} of aniline) at [APS]/[aniline] = 1.25.

$$\mathrm{4nC_6H_5NH_{2(aq)} + 5nS_2O_8{}^{2-}_{(aq)} \rightarrow [(-B{-}NH^{+\cdot}{-}B{-}NH{-})_{2n}](HSO_4{}^-)_{2n(s)} + 6nHSO_4{}^-_{(aq)} + 2nSO_4{}^{2-}_{(aq)}} \quad (11)$$

Morphology of PANISIL Nanocomposites. SEM and TEM images of PANISIL nanocomposites show that their morphology is crucially affected by the initial silica/aniline weight ratio (Figures 5−7). The results of electron microscopy investigations indicate that PANISIL-3 has uniform nanogranular morphology, in contrast to nonuniform morphology of PANISIL-1 and PANISIL-2 which exhibits two types of nanophases: PANI

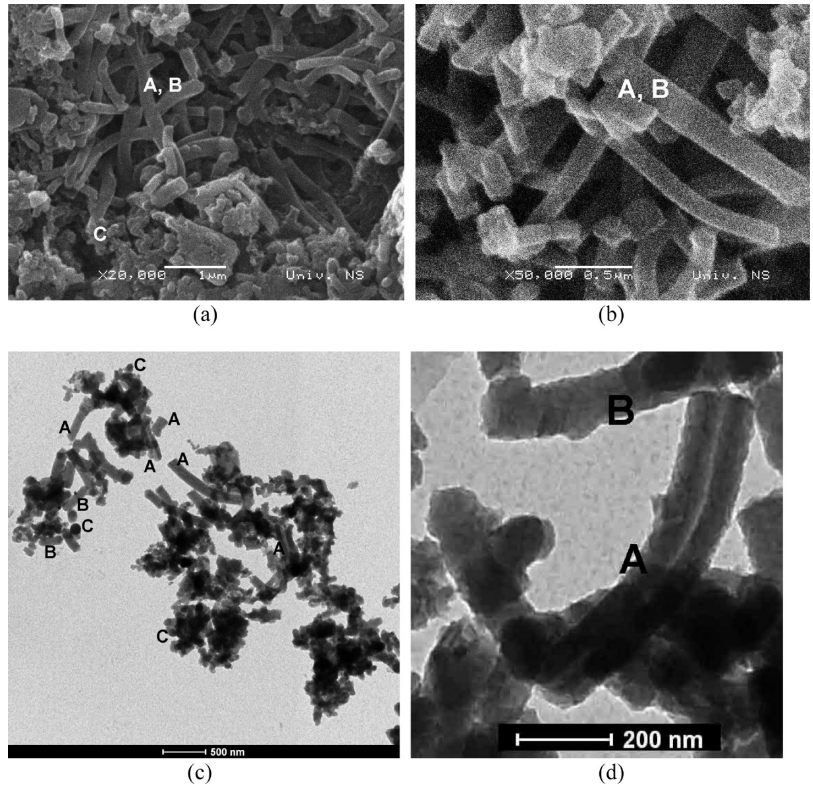

Figure 5. (a,b) SEM and (c,d) TEM images of the sample PANISIL-1 (A, nanotube; B, nanorod; C, nanogranules).

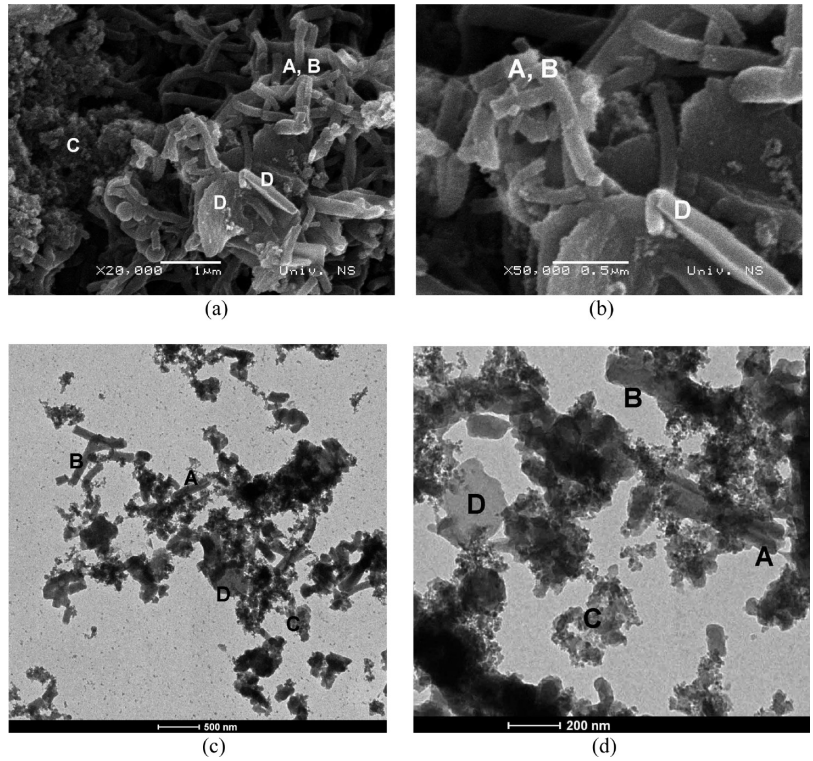

Figure 6. (a,b) SEM and (c,d) TEM images of the sample PANISIL-2 (A, nanotube; B, nanorod; C, nanogranules; D, nanosheet).

nanotubes/nanorods and PANI/silica nanogranules. The content of PANI nanotubes and nanorods is significantly higher in PANISIL-1 than in PANISIL-2. The PANI nanotubes have an average outer diameter of 100−250 nm, an inner diameter of 10−80 nm, and a length extending from 0.2 to 1.5 μm (Figures 5 and 6). Nanotubes are accompanied with nanorods, which have a diameter of 60−100 nm and a length of 0.2−0.7 μm, and PANI/silica nanogranules (Figures 5 and 6). Nanosheets have also been detected by SEM and TEM in the sample PANISIL-2 (Figure 6). The sample PANISIL-3, prepared with the highest amount of colloidal silica, consists of PANI/silica nanogranules with a diameter 35−70 nm, determined by SEM, without the presence of nanocylinders (Figure 7). It should be noted that the pure PANI, synthesized under similar reaction

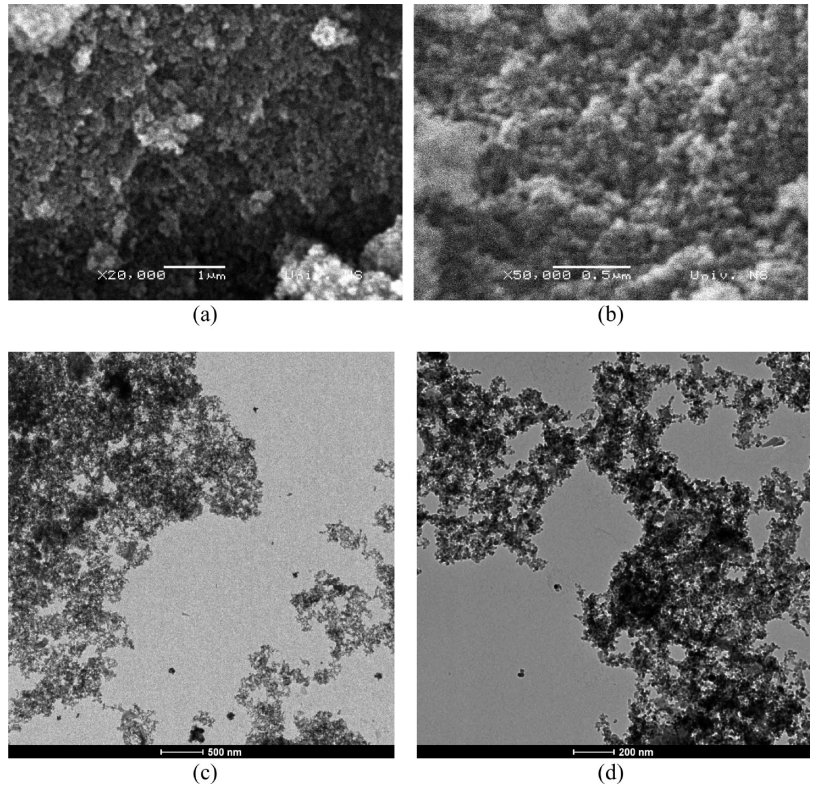

Figure 7. (a,b) SEM and (c,d) TEM images of the sample PANISIL-3.

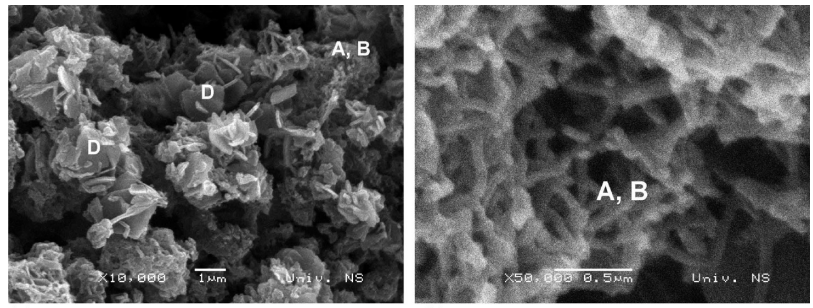

(a) (b)

Figure 8. SEM images of pure PANI, synthesized under the similar reaction conditions as PANISIL composites, without added silica (A, nanotube; B, nanorod; D, nanosheet).

conditions without added colloidal silica, contains nanocylinders of an average diameter 60−100 nm, accompanied with nanosheets, Figure 8.

We proposed that the growth of PANI nanotubes and nanorods occurs in the bulk of the aqueous dispersion of colloidal silica (PANISIL-1 and PANISIL-2). During the first exothermic phase of the oxidative polymerization of aniline in water without added acid, nonprotonated pernigraniline-like and pseudomauveine-like oligoanilines are precipitated as hydrophobic crystallites, which do not adhere efficiently to the hydrophilic surfaces of colloidal silica. The nonconducting needle-like nanocrystallites, with high content of substituted phenazines, which have tendency to build columnar aggregates by stacking,[9] become coated with a conducting PANI hydrogen sulfate film during the third polymerization phase at pH ≤ 2. This leads to the formation of PANI hydrogen sulfate nanorods with nonconducting core and conducting walls. PANI nanotubes are formed by the dissolution of the cores of nanorods,[9] induced by the protonation of fully oxidized oligoanilines at pH ≤ 2. In the case when colloidal silica substantially prevails over aniline (PANISIL-3), the dominant process is oxidative polymerization of adsorbed aniline molecules and the formation of the PANI films on the surface of silica colloidal particles, resulting in the PANI/silica nanogranules composed of silica core and PANI shell.

Thermogravimetric Analysis. The weight ratio of silica/PANI in nanocomposites was determined by thermogravimetric analysis, Figure 9. The main weight loss of the nanocomposites in air stream occurred in the temperature range from ∼300 to 650 °C, attributed to the degradation and decomposition of PANI backbone. Taking into account that the combustion of PANI in air is completed at 650 °C, and the residual weight refers to the content of silica in the nanocomposite, as well as that the weight loss from 25 to 200 °C corresponds to the release of residual water, the weight ratio silica/PANI:

$$w_{\text{silica/PANI}} = \frac{\text{residual mass at 650 °C (\%)}}{\text{residual mass at 200 °C (\%)} - \text{residual mass at 650 °C (\%)}}$$

was determined to amount to 0.05, 0.26, and 2.20 for nanocomposites PANISIL-1, PANISIL-2, and PANISIL-3, respectively. Based on TGA results, content of silica, PANI (in the form of the mixture of sulfate and hydrogen sulfate salts), and water in composites is determined, Table 1. Since the mole ratio $[HSO_4^-]/[SO_4^{2-}] = 2.0$ at pH 1.7, at the end of aniline polymerization, it can be assumed that the mole ratio of PANI hydrogen sulfate $[(-B-NH^{+\bullet}-B-NH-)_{2n}](HSO_4^-)_{2n}$ to PANI sulfate $[(-B-NH^{+\bullet}-B-NH-)_{2n}](SO_4^{2-})_n$, in synthesized PANISIL nanocomposites, is ∼1.

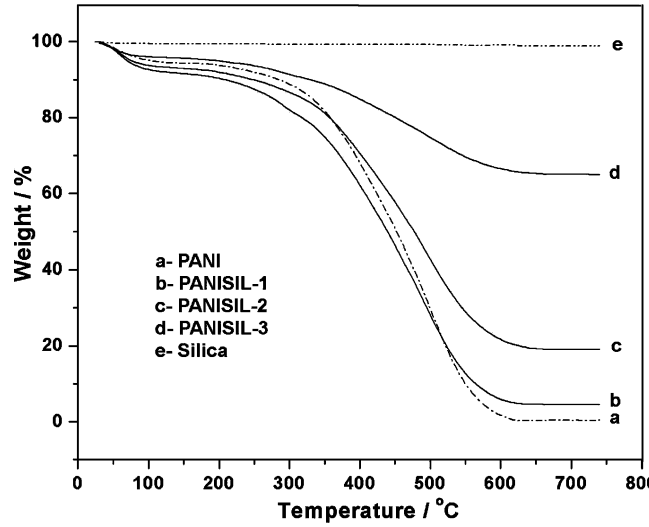

Figure 9. TGA curves for PANISIL-1, PANISIL-2, and PANISIL-3 nanocomposites, pure PANI, and pure colloidal silica, recorded in air stream.

TABLE 1: Content of Silica, PANI (in the Form of the Mixture of Sulfate and Hydrogen Sulfate Salts), and Water in PANISIL Nanocomposites, Determined by TGA

	content (%)		
sample	silica	PANI hydrogen sulfate + PANI sulfate	H_2O
PANISIL-1	4.30	86.02	9.68
PANISIL-2	18.97	72.97	8.06
PANISIL-3	65.25	29.66	5.09

Thermal degradation in nitrogen atmosphere, i.e., carbonization of PANI nanotubes and nanorods in PANISIL-1 nanocomposite, was also studied by TGA (Figure 10). The first weight loss from 30 to ∼200 °C corresponds to the release of residual water. The weight loss in the temperature range from ∼200 to 800 °C is attributed to the release of sulfuric acid from the PANI matrix, followed by the progressive carbonization of PANI. The carbonized PANISIL-1 nanocomposite has the morphology quite similar to that of PANISIL-1, Figure 11. This means that the morphology of PANI nanotubes and nanorods becomes preserved upon the carbonization. The SEM images indicate the presence of carbonized PANI nanotubes which have a rectangular (Figure 11 b) besides the cylindrical cross section.

Elemental Analysis. The elemental composition of PANISIL nanocomposites, found by elemental analysis and ICP-OES measurements (Table 2), shows somewhat higher PANI content (C, N) and lower sulfur content in comparison with corresponding contents calculated on the basis of the content of PANI (supposed to be the equimolar mixture of PANI hydrogen sulfate

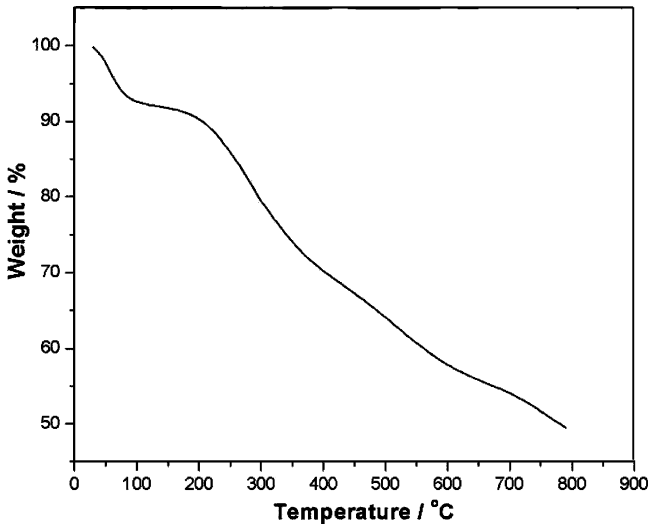

Figure 10. TGA curve for PANISIL-1, recorded under purging nitrogen.

$[C_{24}H_{22}N_4S_2O_8]_n$ and PANI sulfate $[C_{24}H_{20}N_4SO_4]_n$), silica (SiO_2) and water in PANISIL nanocomposites, determined by TGA. These results indicate that the PANI is not in pure emeraldine salt form (PANI hydrogen sulfate/PANI sulfate) in PANISIL nanocomposites, but contains also some undoped emeraldine segments and/or other structural units (phenazine, etc.).

Conductivity. The PANISIL nanocomposites exhibit the electrical conductivity on a semiconductor level, $\sim 10^{-3}-10^{-4}$ S cm^{-1} (Table 3). PANISIL-1 and PANISIL-2 have higher conductivity than pure PANI nanotubes (Table 3). The highest conductivity of PANISIL-2 nanocomposite (4.0×10^{-3} S cm^{-1}) is probably due to the improved self-assembly of the conducting PANI emeraldine salt network in the inorganic matrix combined with the optimum mixed doping effect of nanoparticles, sulfate, and hydrogen sulfate anions. The role of water molecules associated with silica nanoparticles may also be considered. As the weight ratio silica/aniline increases from 0.2 to 2, the conductivity of PANISIL nanocomposite decreases 1 order of magnitude (PANISIL-3). The conductivity of deprotonated nanocomposites is 4−5 orders of magnitude lower ($\sim 10^{-8}$ S cm^{-1}) than that of their protonated forms.

FTIR Spectroscopy. The formation of emeraldine salt form of PANI was proved by the presence of its characteristic bands in the FTIR spectra of all PANISIL nanocomposites (Figure 12). The FTIR spectra of PANISIL nanocomposites exhibit main PANI emeraldine salt bands at $\sim$1580−1570 cm^{-1} and $\sim$1493 cm^{-1}, assigned to quinonoid (Q) and benzenoid (B) ring-stretching, respectively.[9,18,60] These bands show a blue shift to $\sim$1590 and $\sim$1504 cm^{-1} in the spectra of deprotonated

TABLE 2: Elemental Composition of PANISIL Nanocomposites Determined by the Elemental Analysis (C, H, N, and S), ICP-OES Measurements (Si), and by Difference (O), and the Elemental Composition Calculated on the Basis of the Content of PANI (the Equimolar Mixture of PANI Sulfate and PANI Hydrogen Sulfate), Silica, and Water in PANISIL Nanocomposites (Determined by TGA)

		content (%)					
sample		C	H	N	S	Si	O (by diff)
PANISIL-1	calculated	48.66	4.67	9.46	8.12	2.01	27.08
	found	55.71	4.64	11.04	5.20	0.83	22.58
PANISIL-2	calculated	41.27	3.94	8.02	6.89	8.87	31.01
	found	46.65	3.96	9.13	4.21	7.90	28.15
PANISIL-3	calculated	16.78	1.80	3.26	2.80	30.50	44.86
	found	17.29	1.74	3.69	2.32	28.52	46.44

TABLE 3: Conductivity of Protonated, PANISIL, and Deprotonated, PANISIL-D, Nanocomposites

protonated sample	conductivity of protonated sample (S cm^{-1})	deprotonated sample	conductivity of deprotonated sample (S cm^{-1})
PANI	2.1×10^{-3}	–	–
PANISIL-1	3.3×10^{-3}	PANISIL-D-1	1.8×10^{-8}
PANISIL-2	4.0×10^{-3}	PANISIL-D-2	1.4×10^{-8}
PANISIL-3	5.5×10^{-4}	PANISIL-D-3	1.1×10^{-8}

PANISIL-D nanocomposites, typical for transformation of emeraldine salt to emeraldine base form (Figure 13). The band observed at 1379 cm^{-1} in the spectra of all PANISIL-D nanocomposites is due to the C−N stretching vibration in the segment $QB_{trans}Q$, which is characteristic for the PANI emeraldine base.[60] The band at 1300−1308 cm^{-1} observed in the spectra of all samples, protonated as well as deprotonated, corresponds to the C−N stretching of secondary aromatic amine. The significant blue shift of the PANI bands at 1568 and 1302 cm^{-1} (PANISIL-1 and PANISIL-2) to 1581 and 1308 cm^{-1} (PANISIL-3), respectively, indicates strengthening of interactions between PANI chains and silica with the increase of the initial silica/aniline weight ratio. This feature is well correlated with the change in morphology of nanocomposites. Analogous blue shift is also present, but less marked in the spectra of deprotonated nanocomposites. The FTIR spectra of all protonated PANISIL nanocomposites show the band at $\sim$1244 cm^{-1}, which is attributed to the C−NH$^{\cdot+}$ stretching, characteristic of polaron form of PANI emeraldine salt.[9] The prominent band at $\sim$1146 cm^{-1} in the spectra of PANISIL-1 and PANISIL-2 nanocomposites is assigned to the stretching vibration of $-NH^+=$ (in the B−NH$^+$=Q segment) in bipolaron form of PANI emeraldine salt.[61] The bands at $\sim$1244 and $\sim$1146 cm^{-1} are still present, although weakened, in the spectra of deprotonated PANISIL-D-1 and PANISIL-D-2 samples, indicating significant interactions NH$^{\cdot+}$---$^-$O−Si$^+$ and NH$^+$---$^-$O−Si$^+$

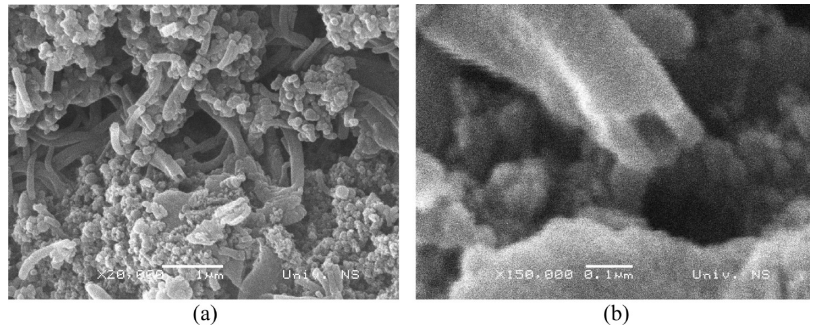

(a) (b)

Figure 11. (a,b) SEM images of the product of carbonization of sample PANISIL-1 in nitrogen stream up to 800 °C.

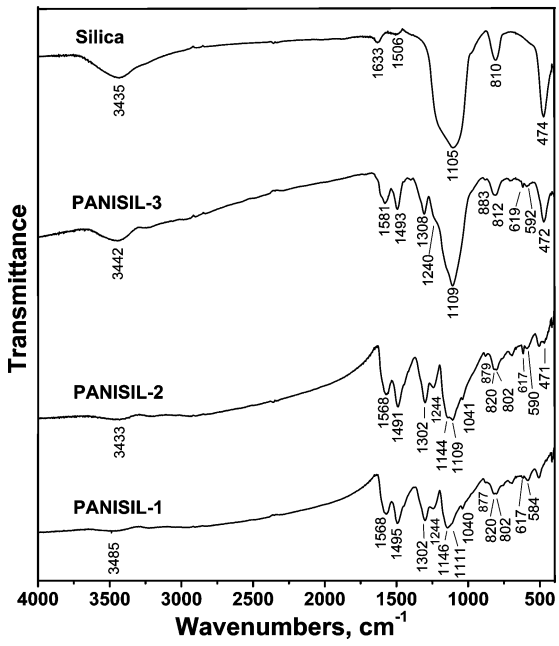

Figure 12. FTIR spectra of PANISIL nanocomposites and anhydrous colloidal silica which was used in the syntheses.

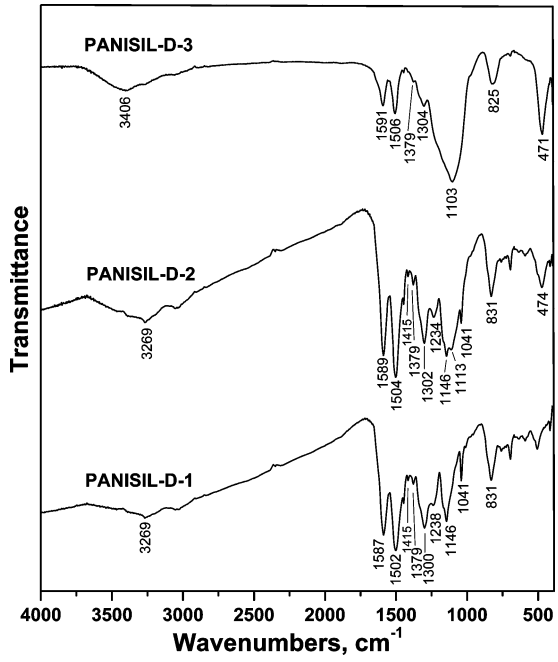

Figure 13. FTIR spectra of PANISIL-D nanocomposites.

between PANI and silica which stabilize PANI polaron and bipolaron structure, respectively, at PANI/silica interface in the deprotonated samples. Hydrogen sulfate counterion is evidenced in the spectra of PANISIL-1 and PANISIL-2 by the bands at 1040 cm^{-1} (symmetric SO_3 stretching), ~880 cm^{-1} (probably S−OH stretching), and ~617 and ~590 cm^{-1}.[18,61] A contribution of asymmetric SO_3 stretching vibration in hydrogen sulfate anion to the band at ~1146 cm^{-1} is also possible. In the spectrum of PANISIL-3, the bands at ~1146 and 1040 cm^{-1} are probably masked by very strong band of silica located at 1109 cm^{-1}. The bands at 820 and ~830 cm^{-1} for PANISIL and PANISIL-D samples, respectively, are due to the aromatic C−H out-of-plane deformation vibration of 1,4-disubstituted benzene ring in linear N−C4 coupled PANI chains.[9,18,60,61]

Besides the bands of standard PANI, the band at 1415 cm^{-1} is observed in the FTIR spectra of the samples PANISIL-D-1

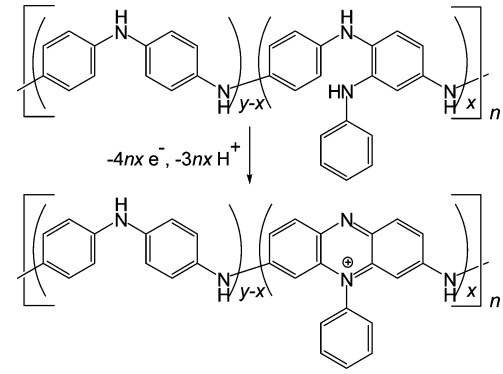

Figure 14. Formation of substituted phenazine units in PANI.

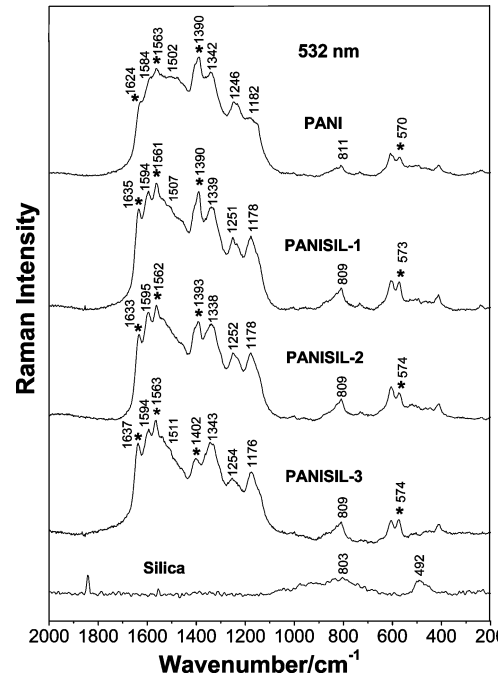

Figure 15. Raman spectra of PANISIL nanocomposites, PANI, and anhydrous colloidal silica, at excitation wavelength of 532 nm. Bands marked with (*) are assigned to substituted phenazine segments.

and PANISIL-D-2 (Figure 13), which is attributed to the substituted phenazine units, formed by the oxidative intramolecular cyclization of branched oligoaniline and PANI chains (Figure 14).[18] Phenazine units have an important role in the formation of nanocylindrical morphology of PANI.[9,12,13,18,46−48,57]

The bands which appear at 1105, 810, and 474 cm^{-1} in the FTIR spectrum of pure colloidal silica (Figure 12) due to the asymmetrical stretching vibration, the symmetrical stretching vibration, and the rocking deformation vibration of Si−O−Si, respectively,[62,63] are present also in the spectra of all PANISIL nanocomposites. Relative intensity of the silica bands increases with increase of the initial silica/aniline weight ratio. These bands are shifted in the spectra of PANISIL nanocomposites to 1111 cm^{-1} (PANISIL-1), 1109 cm^{-1} (PANISIL-2 and PANISIL-3), 802 cm^{-1} (PANISIL-1 and PANISIL-2), 812 cm^{-1} (PANISIL-3), 470 cm^{-1} (PANISIL-2), and 472 cm^{-1} (PANISIL-3). All these shifts indicate the significant interaction between PANI chains and silica.

Raman Spectroscopy. The most important feature observed in the Raman spectra of PANISIL nanocomposites (Figure 15) is the presence of bands at 1637−1633, 1563−1561, 1402−1390, and 574 cm^{-1} associated with substituted phenazine structural units,[9,50,51,57,64] crucially important for the formation of the

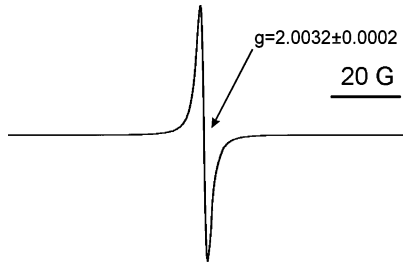

Figure 16. EPR spectrum of PANISIL-3 nanocomposite, measured at room temperature.

nanostructured PANI morphology.[9,12,13,18,46−48,57] In the Raman spectrum of pure PANI these bands are located at 1624, 1563, 1390, and 570 cm^{-1}. A comparison of the spectra of PANISIL nanocomposites reveals that the band at 1390 cm^{-1} is relatively strongest in the spectrum of PANISIL-1, and it shows a decrease in intensity as well as a shift to higher wavenumbers (1393 cm^{-1} for PANISIL-2, 1402 cm^{-1} for PANISIL-3) with increasing the content of silica in PANISIL samples. The Raman bands attributed to PANI emeraldine salt segments are observed for all PANISIL samples at ∼1594 cm^{-1} (the C∼C stretching vibration of the semiquinonoid (SQ) ring, where "∼" denotes the bond intermediate between the single and double bond), 1511−1507 cm^{-1} (the N−H deformation vibration of protonated amine), 1343−1338 cm^{-1} (the C∼$N^{\cdot+}$ stretching vibration of delocalized polaronic structures), and 1176−1178 cm^{-1} (the C−H bending in-plane vibration of SQ ring).[9,57] The band attributed to C−N stretching of benzenoid ring, positioned at 1246 cm^{-1} in the spectrum of pure PANI, shows a blue shift to 1251 cm^{-1} (PANISIL-1), 1252 cm^{-1} (PANISIL-2), and 1254 cm^{-1} (PANISIL-3) with increase of silica content. The Raman bands of colloidal silica at 804 and 492 cm^{-1} coincide with PANI bands at 809 cm^{-1} (out-of-plane C−H deformation of quinonoid ring, ring deformation of SQ ring and/or out-of-plane C−H wagging)[57] and ∼495−492 cm^{-1} (phenazine-like segment),[57] respectively.

EPR Spectroscopy. All PANISIL nanocomposites show EPR signals which confirm the existence of cation radicals in the macromolecular chains. Pure PANI and all PANISIL nanocomposites have the symmetric EPR signals with the shape similar to that shown for PANISIL-3 in Figure 16. For all PANISIL nanocomposites the EPR *g*-value is determined to amount 2.0032. The EPR peak area, relative to pure PANI, substantially decreases with increasing silica content in order 1.53, 1.23, and 0.60 for the samples PANISIL-1, PANISIL-2, and PANISIL-3, respectively. The result that the nanocomposites PANISIL-1 and PANISIL-2 show higher EPR peak area compared with pure PANI correlates well with the conductivity data. Colloidal silica itself has no EPR signal.

Conclusions

We have demonstrated an efficient template-free method for the synthesis of novel conducting polyaniline nanotubes/silica nanocomposites, through the oxidative polymerization of aniline with ammonium peroxydisulfate in aqueous dispersions of colloidal silica without added acid. This simple and versatile synthetic method could be extended to prepare a wide range of other nanocomposites of conducting self-assembled polyaniline nanotubes and various inorganic materials.

The initial silica/aniline weight ratio has crucial influence on the kinetics and thermochemistry of aniline polymerization, as well as on the morphology of synthesized polyaniline/silica nanocomposites. The syntheses of polyaniline nanotubes/silica nanocomposites, using the initial silica/aniline weight ratio ≤0.2, proceed in two exothermic phases which are well separated by an athermal period, while the synthesis of polyaniline/silica nanogranules, at silica/aniline weight ratio ∼2, proceeds as an complex exothermic process, i.e., two rapid heat evolutions intercepted with slow heat evolution. The oxidative polymerization of aniline in aqueous dispersions of colloidal silica is completed considerably faster than in water without added colloidal silica. Because of the adsorption of aniline molecules on colloidal silica particles, leading to the decrease of the concentration of aniline molecules in the bulk of the aqueous silica dispersion, the presence of colloidal silica causes the decrease of both the initial rate of aniline oxidation and the amount of heat released during the first exothermic phase of aniline polymerization. The substantial increase of the surface area of precipitated oligoanilines in the presence of colloidal silica causes a significant acceleration of redox reactions during the second polymerization phase, i.e., the much shorter athermal periods during syntheses of polyaniline nanotubes/silica nanocomposites, in comparison with the corresponding athermal period of synthesis of pure polyaniline nanotubes, in water without added acid.

The polyaniline nanotubes have an average outer diameter of 100−250 nm, an inner diameter of 10−80 nm, and a length extending from 0.2 to 1.5 μm. Nanotubes are accompanied with nanorods, which have a diameter of 60−100 nm and a length of 0.2−0.7 μm, nanosheets, and polyaniline/silica nanogranules. The morphology of polyaniline nanotubes/silica nanocomposites becomes preserved upon the carbonization. The nanocomposite prepared with the highest amount of colloidal silica (silica/aniline weight ratio ∼2) has uniform morphology composed of polyaniline/silica nanogranules with a diameter 35−70 nm, without the presence of nanocylinders.

Polyaniline nanotubes/silica nanocomposites show conductivity in the range (3.3−4.0) × 10^{-3} S cm^{-1}, paramagnetic properties (g = 2.0032), and emeraldine oxidation state with the presence of substituted phenazine units, proved by FTIR and Raman spectroscopies. These novel nanostructured composites, which combine unique properties of 1D polyaniline nanostructures and polyaniline/colloidal silica hybrid materials, could be applied as electronic components and catalysts.

Acknowledgment. The authors thank the Ministry of Science and Technological Development of Serbia (contract no. 142047) and Grant Agency of the Academy of Sciences of the Czech Republic (IAA 400500905) for financial support.

References and Notes

(1) Stejskal, J.; Gilbert, R. G. *Pure Appl. Chem.* **2002**, *74*, 857.
(2) Chiang, J.-C.; MacDiarmid, A. G. *Synth. Met.* **1986**, *13*, 193.
(3) (a) MacDiarmid, A. G.; Yang, L. S.; Huang, W.-S.; Humphrey, B. D. *Synth. Met.* **1987**, *18*, 393. (b) McCall, R. P.; Ginder, J. M.; Leng, J. M.; Coplin, K. A.; Ye, H. J.; Epstein, A. J.; Asturias, G. E.; Manohar, S. K.; Masters, J. G.; Scherr, E. M.; Sun, Y.; MacDiarmid, A. G. *Synth. Met.* **1991**, *41*, 1329. (c) Trivedi, D. C.; Dhawan, S. K. *Synth. Met.* **1993**, *59*, 267. (d) Makeiff, D. A.; Huber, T. *Synth. Met.* **2006**, *156*, 497. (e) Dutta, D.; Sarma, T. K.; Chowdhury, D.; Chattopadhyay, A. *J. Colloid Interface Sci.* **2005**, *283*, 153. (f) Drelinkiewicz, A.; Waksmundzka-Góra, A.; Sobczak, J. W.; Stejskal, J. *Appl. Catal. A: Gen.* **2007**, *333*, 219. (g) Zhao, C.; Xing, S.; Yu, Y.; Zhang, W.; Wang, C. *Microelectron. J.* **2007**, *38*, 316. (h) Willner, I.; Willner, B.; Katz, E. *Bioelectrochemistry* **2007**, *70*, 2.
(4) (a) Blinova, N. V.; Stejskal, J.; Trchová, M.; Ćirić-Marjanović, G.; Sapurina, I. *J. Phys. Chem. B* **2007**, *111*, 2440. (b) Sun, L.-J.; Liu, X.-X.; Lau, K. K.-T.; Chen, L.; Gu, W.-M. *Electrochim. Acta* **2008**, *53*, 3036. (c) Bessière, A.; Duhamel, C.; Badot, J.-C.; Lucas, V.; Certiat, M.-C. *Electrochim. Acta* **2004**, *49*, 2051. (d) Halvorson, C.; Cao, Y.; Moses, D.; Heeger, A. J. *Synth. Met.* **1993**, *57*, 3941. (e) Wang, H. L.; MacDiarmid, A. G.; Wang, Y. Z.; Gebler, D. D.; Epstein, A. J. *Synth. Met.* **1996**, *78*, 33.

(f) Kaneto, K.; Kaneko, M.; Min, Y.; MacDiarmid, A. G. *Synth. Met.* **1995**, *71*, 2211. (g) Soto-Oviedo, M. A.; Araújo, O. A.; Faez, R.; Rezende, M. C.; De Paoli, M.-A. *Synth. Met.* **2006**, *156*, 1249. (h) Kalendová, A.; Veselý, D.; Stejskal, J. *Prog. Org. Coat.* **2008**, *62*, 105.

(5) Stejskal, J.; Kratochvíl, P.; Jenkins, A. D. *Polymer* **1996**, *37*, 367.

(6) (a) Virji, S.; Huang, J.; Kaner, R. B.; Weiller, B. H. *Nano Lett.* **2004**, *4*, 491. (b) Huang, J. *Pure Appl. Chem.* **2006**, *78*, 15.

(7) (a) Zhang, Z.; Wei, Z.; Wan, M. *Macromolecules* **2002**, *35*, 5937. (b) Lu, X.; Mao, H.; Chao, D.; Zhang, W.; Wei, Y. *Macromol. Chem. Phys.* **2006**, *207*, 2142.

(8) (a) Qiu, H.; Wan, M. *J. Polym. Sci. A: Polym. Chem.* **2001**, *39*, 3485. (b) Qiu, H.; Wan, M.; Matthews, B.; Dai, L. *Macromolecules* **2001**, *34*, 675. (c) Zhang, L.; Wan, M. *Nanotechnology* **2002**, *13*, 750. (d) Wei, Z.; Zhang, Z.; Wan, M. *Langmuir* **2002**, *18*, 917. (e) Long, Y.; Zhang, L.; Ma, Y.; Chen, Z.; Wang, N.; Zhang, Z.; Wan, M. *Macromol. Rapid Commun.* **2003**, *24*, 938. (f) Long, Y.; Luo, J.; Xu, J.; Chen, Z.; Zhang, L.; Li, J.; Wan, M. *J. Phys.: Condens. Matter* **2004**, *16*, 1123. (g) Xia, H.; Chan, H. S. O.; Xiao, C.; Cheng, D. *Nanotechnology* **2004**, *15*, 1807. (h) Pinto, N. J.; Carrión, P. L.; Ayala, A. M.; Ortiz-Marciales, M. *Synth. Met.* **2005**, *148*, 271. (i) Zhang, Z.; Wei, Z.; Zhang, L.; Wan, M. *Acta Mater.* **2005**, *53*, 1373. (j) Zhang, L.; Wan, M. *Thin Solid Films* **2005**, *477*, 24. (k) Xia, H.; Narayanan, J.; Cheng, D.; Xiao, C.; Liu, X.; Chan, H. S. O. *J. Phys. Chem. B* **2005**, *109*, 12677.

(9) Janošević, A.; Ćirić-Marjanović, G.; Marjanović, B.; Holler, P.; Trchová, M.; Stejskal, J. *Nanotechnology* **2008**, *19*, 135606.

(10) (a) Yang, Y. S.; Wan, M. X. *J. Mater. Chem.* **2002**, *12*, 897. (b) Zhang, L.; Wan, M. *Adv. Funct. Mater.* **2003**, *13*, 815. (c) Zhang, L.; Long, Y.; Chen, Z.; Wan, M. *Adv. Funct. Mater.* **2004**, *14*, 693. (d) Zhang, L.; Peng, H.; Zujovic, Z. D.; Kilmartin, P. A.; Soeller, C.; Travas-Sejdic, J. *Macromol. Chem. Phys.* **2007**, *208*, 1210. (e) Sun, Q.; Deng, Y. *Mater. Lett.* **2008**, *62*, 1831. (f) Zujovic, Z. D.; Zhang, L.; Bowmaker, G. A.; Kilmartin, P. A.; Travas-Sejdic, J. *Macromolecules* **2008**, *41*, 3125. (g) Petrov, P.; Mokreva, P.; Tsvetanov, C.; Terlemezyan, L. *Colloid Polym. Sci.* **2008**, *286*, 691. (h) Sun, Q.; Park, M.-C.; Deng, J. *Mater. Chem. Phys.* **2008**, *110*, 276.

(11) Konyushenko, E. N.; Stejskal, J.; Šeděnková, I.; Trchová, M.; Sapurina, I.; Cieslar, M.; Prokeš, J. *Polym. Int.* **2006**, *55*, 31.

(12) Stejskal, J.; Sapurina, I.; Trchová, M.; Konyushenko, E. N.; Holler, P. *Polymer* **2006**, *47*, 8253.

(13) Stejskal, J.; Sapurina, I.; Trchová, M.; Konyushenko, E. N. *Macromolecules* **2008**, *41*, 3530.

(14) (a) Zhang, L.; Peng, H.; Hsu, C. F.; Kilmartin, P. A.; Travas-Sejdic, J. *Nanotechnology* **2007**, *18*, 115607. (b) Zhang, L.; Peng, H.; Kilmartin, P. A.; Soeller, C.; Travas-Sejdic, J. *Electroanalysis* **2007**, *19*, 870. (c) Zhang, L.; Peng, H.; Sui, J.; Kilmartin, P. A.; Travas-Sejdic, J. *Curr. Appl. Phys.* **2008**, *8*, 312.

(15) Wei, Z.; Wan, M.; Lin, T.; Dai, L. *Adv. Mater.* **2003**, *15*, 136.

(16) Cheng, C.; Jiang, J.; Tang, R.; Xi, F. *Synth. Met.* **2004**, *145*, 61.

(17) Zhang, L.; Wan, M. *J. Phys. Chem. B* **2003**, *107*, 6748.

(18) Trchová, M.; Konyushenko, E. N.; Stejskal, J.; Šeděnková, I.; Holler, P.; Ćirić-Marjanović, G. *J. Phys. Chem. B* **2006**, *110*, 9461.

(19) (a) Chiou, N.-R.; Lee, L. J.; Epstein, A. J. *Chem. Mater.* **2007**, *19*, 3589. (b) Ding, H.; Shen, J.; Wan, M.; Chen, Z. *Macromol. Chem. Phys.* **2008**, *209*, 864.

(20) (a) Armes, S. P.; Gottesfeld, S.; Beery, J. G.; Garzon, F.; Agnew, S. F. *Polymer* **1991**, *32*, 2325. (b) Gill, M.; Mykytiuk, J.; Armes, S. P.; Edwards, J. L.; Yeates, T.; Moreland, P. J.; Mollet, C. *J. Chem. Soc., Chem. Commun.* **1992**, 108. (c) Gill, M.; Armes, S. P.; Fairhurst, D.; Emmett, S. N.; Idzorek, G.; Pigott, T. *Langmuir* **1992**, *8*, 2178. (d) Terrill, N. J.; Crowley, T.; Gill, M.; Armes, S. P. *Langmuir* **1993**, *9*, 2093. (e) Gill, M.; Baines, F. L.; Armes, S. P. *Synth. Met.* **1993**, *55*−*57*, 1029. (f) Flitton, R.; Johal, J.; Maeda, S.; Armes, S. P. *J. Colloid Interface Sci.* **1995**, *173*, 135. (g) Butterworth, M. D.; Corradi, R.; Johal, J.; Lascelles, S. F.; Maeda, S.; Armes, S. P. *J. Colloid Interface Sci.* **1995**, *174*, 510.

(21) Wei, Y.; Yeh, J.; Jin, D.; Jia, X.; Wang, J. *Chem. Mater.* **1995**, *7*, 969.

(22) (a) Stejskal, J.; Kratochvíl, P.; Armes, S. P.; Lascelles, S. F.; Riede, A.; Helmstedt, M.; Prokeš, J.; Křivka, I. *Macromolecules* **1996**, *29*, 6814. (b) Riede, A.; Helmstedt, M.; Riede, V.; Stejskal, J. *Colloid Polym. Sci.* **1997**, *275*, 814. (c) Gill, M. T.; Chapman, S. E.; DeArmitt, C. L.; Baines, F. L.; Dadswell, C. M.; Stamper, J. G.; Lawless, G. A.; Billingham, N. C.; Armes, S. P. *Synth. Met.* **1998**, *93*, 227. (d) Riede, A.; Helmstedt, M.; Riede, V.; Stejskal, J. *Langmuir* **1998**, *14*, 6767. (e) Huang, S. W.; Neoh, K. G.; Kang, E. T.; Han, H. S.; Tan, K. L. *J. Mater. Chem.* **1998**, *8*, 1743.

(23) Aboutanos, V.; Barisci, J. N.; Kane-Maguire, L. A. P.; Wallace, G. G. *Synth. Met.* **1999**, *106*, 89.

(24) Neoh, K. G.; Tan, K. K.; Goh, P. L.; Huang, S. W.; Kang, E. T.; Tan, K. L. *Polymer* **1999**, *40*, 887.

(25) Riede, A.; Helmstedt, M.; Riede, V.; Zemek, J.; Stejskal, J. *Langmuir* **2000**, *16*, 6240.

(26) (a) Stejskal, J.; Sulimenko, T.; Prokeš, J.; Sapurina, I. *Colloid Polym. Sci.* **2000**, *278*, 654. (b) Trlica, J.; Sáha, P.; Quadrat, O.; Stejskal, J. *J. Phys. D: Appl. Phys.* **2000**, *33*, 1773.

(27) (a) Jang, S. H.; Han, M. G.; Im, S. S. *Synth. Met.* **2000**, *110*, 17. (b) Wang, Y.; Wang, X.; Li, J.; Mo, Z.; Zhao, X.; Jing, X.; Wang, F. *Adv. Mater.* **2001**, *13*, 1582.

(28) (a) Riede, A.; Stejskal, J.; Helmstedt, M. *Synth. Met.* **2001**, *121*, 1365. (b) Stejskal, J. *J. Polym. Mater.* **2001**, *18*, 225.

(29) Neves, S.; Fonseca, C. P. *J. Power Sources* **2002**, *107*, 13.

(30) Niu, Z.; Yang, Z.; Hu, Z.; Lu, Y.; Han, C. C. *Adv. Funct. Mater.* **2003**, *13*, 949.

(31) Stejskal, J.; Trchová, M.; Fedorova, S.; Sapurina, I.; Zemek, J. *Langmuir* **2003**, *19*, 3013.

(32) Neves, S.; Fonseca, C. P. *J. Braz. Chem. Soc.* **2004**, *15*, 395.

(33) Takei, T.; Yoshimura, K.; Yonesaki, Y.; Kumada, N.; Kinomura, N. *J. Porous Mater.* **2005**, *12*, 337.

(34) Widera, J.; Kijak, A. M.; Ca, D. V.; Pacey, G. E.; Taylor, R. T.; Perfect, H.; Cox, J. A. *Electrochim. Acta* **2005**, *50*, 1703.

(35) Feng, X.; Yang, G.; Liu, Y.; Hou, W.; Zhu, J.-J. *J. Appl. Polym. Sci.* **2006**, *101*, 2088.

(36) Nastase, F.; Stamatin, I.; Nastase, C.; Mihaiescu, D.; Moldovan, A. *Prog. Solid State Chem.* **2006**, *34*, 191.

(37) (a) Jang, J.; Ha, J.; Lim, B. *Chem. Commun.* **2006**, 1622. (b) Dutta, K.; De, S. K. *J. Nanosci. Nanotechnol.* **2006**, *6*, 499.

(38) Hwang, T.; Quilitz, M.; Schmidt, H. *J. New Mater. Electrochem. Systems* **2007**, *10*, 237.

(39) Dutta, K.; De, S. K. *Phys. Lett. A* **2007**, *361*, 141.

(40) Chen, C.-Y.; Garnica-Rodriguez, J. I.; Duke, M. C.; Dalla Costa, R. F.; Dicks, A. L.; Diniz da Costa, J. C. *J. Power Sources* **2007**, *166*, 324.

(41) Lei, X.; Su, Z. *Polym. Adv. Technol.* **2007**, *18*, 472.

(42) Shim, G. H.; Han, M. G.; Sharp-Norton, J. C.; Creager, S. E.; Foulger, S. H. *J. Mater. Chem.* **2008**, *18*, 594.

(43) Liu, X. X.; Li, Y. B.; Bian, L. J.; Dou, Y. Q.; Huo, Y. Q. *J. Solid State Electrochem.* **2008**, *12*, 909.

(44) Lee, H.-T.; Wang, C.-C. *Polym. Eng. Sci.* **2008**, *48*, 439.

(45) Kim, T. H.; Kim, Y.; Lee, S. J.; Han, W. S.; Jung, J. H. *Chem. Lett.* **2008**, *37*, 598.

(46) Ćirić-Marjanović, G.; Trchová, M.; Stejskal, J. *Collect. Czech. Chem. Commun.* **2006**, *71*, 1407.

(47) Ćirić-Marjanović, G.; Trchová, M.; Stejskal, J. *Int. J. Quantum Chem.* **2008**, *108*, 318.

(48) Ćirić-Marjanović, G.; Konyushenko, E. N.; Trchová, M.; Stejskal, J. *Synth. Met.* **2008**, *158*, 200.

(49) Ćirić-Marjanović, G.; Trchová, M.; Matějka, P.; Holler, P.; Marjanović, B.; Juranić, I. *React. Funct. Polym.* **2006**, *66*, 1670.

(50) Ćirić-Marjanović, G.; Blinova, N. V.; Trchová, M.; Stejskal, J. *J. Phys. Chem. B* **2007**, *111*, 2188.

(51) Ćirić-Marjanović, G.; Trchová, M.; Konyushenko, E. N.; Holler, P.; Stejskal, J. *J. Phys. Chem. B* **2008**, *112*, 6976.

(52) Stewart, J. J. P. *J. Comput. Chem.* **1989**, *10*, 209.

(53) Stewart, J. J. P. *J. Comput.-Aided Mol. Des.* **1990**, *4*, 1.

(54) (a) Banerjee, A.; Adams, N.; Simons, J.; Shepard, R. *J. Phys. Chem.* **1985**, *89*, 52. (b) Baker, J. *J. Comput. Chem.* **1986**, *7*, 385.

(55) Burkert, U.; Allinger, N. L. *Molecular Mechanics*; American Chemical Society: Washington, DC, 1982.

(56) Klamt, A.; Schüürmann, G. *J. Chem. Soc., Perkin Trans.* **1993**, *2*, 799.

(57) Ćirić-Marjanović, G.; Trchová, M.; Stejskal, J. *J. Raman Spectrosc.* **2008**, *39*, 1375.

(58) Gospodinova, N.; Terlemezyan, L. *Prog. Polym. Sci.* **1998**, *23*, 1443.

(59) Fu, Y.; Elsenbaumer, R. L. *Chem. Mater.* **1994**, *6*, 671.

(60) Kang, E. T.; Neoh, K. G.; Tan, K. L. *Prog. Polym. Sci.* **1998**, *23*, 277.

(61) Socrates, G. *Infrared and Raman Characteristic Group Frequencies: Tables and Charts*; Wiley: New York, 2001; pp 107−109, 157−165.

(62) Martinez, J. R.; Ruiz, F.; Vorobiev, Y. V.; Perez-Robles, F.; Gonzales-Hernandez, J. *Chem. Phys.* **1998**, *109*, 7511.

(63) Lenza, R. F. S.; Vasconcelos, W. L. *Mater. Res.* **2002**, *5*, 497.

(64) do Nascimento, G. M.; Silva, C. H. B.; Temperini, M. L. A. *Macromol. Rapid Commun.* **2006**, *27*, 255.

JP900096B